High-efficiency InGaN/AlInGaN multiple quantum wells with lattice-matched AlInGaN superlattices barrier*

Feng Xu(徐峰)[1,2], Peng Chen(陈鹏)[1,2,†], Fu-Long Jiang(蒋府龙)[1], Ya-Yun Liu(刘亚云)[1], Zi-Li Xie(谢自立)[1], Xiang-Qian Xiu(修向前)[1], Xue-Mei Hua(华雪梅)[1], Yi Shi(施毅)[1], Rong Zhang(张荣)[1], and You-Liao Zheng(郑有炓)[1]

[1] *Key Laboratory of Advanced Photonic and Electronic Materials, School of Electronic Science and Engineering, Nanjing University, Nanjing* 210093, *China*

[2] *Nanjing University Institute of Optoelectronics at Yangzhou, Yangzhou* 225009, *China*

(Received 22 July 2016; revised manuscript received 18 October 2016; published online 22 December 2016)

A new approach to fabricating high-quality AlInGaN film as a lattice-matched barrier layer in multiple quantum wells (MQWs) is presented. The high-quality AlInGaN film is realized by growing the AlGaN/InGaN short period superlattices through metalorganic chemical vapor deposition, and then being used as a barrier in the MQWs. The crystalline quality of the MQWs with the lattice-matched AlInGaN barrier and that of the conventional InGaN/GaN MQWs are characterized by x-ray diffraction and scanning electron microscopy. The photoluminescence (PL) properties of the InGaN/AlInGaN MQWs are investigated by varying the excitation power density and temperature through comparing with those of the InGaN/GaN MQWs. The integral PL intensity of InGaN/AlInGaN MQWs is over 3 times higher than that of InGaN/GaN MQWs at room temperature under the highest excitation power. Temperature-dependent PL further demonstrates that the internal quantum efficiency of InGaN/AlInGaN MQWs (76.1%) is much higher than that of InGaN/GaN MQWs (21%). The improved luminescence performance of InGaN/AlInGaN MQWs can be attributed to the distinct reduction of the barrier-well lattice mismatch and the strain-induced non-radiative recombination centers.

Keywords: AlInGaN superlattices, MQWs, photoluminescence, x-ray diffraction spectrum

PACS: 78.55.Cr, 78.67.Pt, 78.67.De, 78.55.–m **DOI:** 10.1088/1674-1056/26/1/017803

1. Introduction

The $Al_xIn_yGa_{1-x-y}N$ quaternary alloy system has attracted intense attention because its band gap and lattice constant is allowed to be independently adjusted by tuning Al or In composition.[1–4] Furthermore, owing to the higher thermal stability, using AlInGaN as the protection layer is effective to suppress the generation of non-radiative recombination centers in multiple quantum wells (MQWs) caused by thermal damage in the ramp-up process of metalorganic chemical vapor deposition (MOCVD).[5] Accordingly, AlInGaN is an ideal material for minimizing mismatch-induced strain and enhancing band offset in GaN-based heterostructure.[6]

At present, most researchers concentrate on the enhanced luminescence efficiency for InGaN-based MQWs with different polarization-matched barriers.[2,7,8] For group-III nitrides, the built-in electrostatic fields related to the spontaneous and piezoelectric polarizations affect strongly the optical properties of the MQWs.[8–10] For strain-free purposes, the use of a lattice-matched AlInGaN barrier layer is proposed. Although AlInGaN has many unique advantages, there are several epitaxial issues when it is prepared by the conventional preparation method: (i) rigorous growth condition (growth temperature, growth rate, V/III flux ratio, etc.),[11,12] (ii) spatial compositional (or strain) fluctuation or disordering, and (iii) compositional pulling effect. For case (i), In atoms tend to form clusters because the In atom size is much bigger than Ga and Al atoms. Moreover, InN requires much lower growth temperature than AlN.[13] Thus, it is difficult to realize the optimal growth condition for incorporating In atoms into AlInGaN homogeneously and avoiding the phenomena of phase separation. In addition, cases (ii) and (iii) become dominant with increasing epilayer thickness, which will make the Al/In ratio deviate from lattice match, thereby degrading crystal quality by introducing the hexagonal-opening (i.e., V-shaped) pits onto the AlInGaN surface.[14,15] All of these cases mentioned above restrict the applications of AlInGaN material in such MQWs optoelectronic devices as light-emitting diodes and laser diodes.

In this paper, we present a new process for fabricating high-quality AlInGaN by using the AlGaN/InGaN short period superlattices. Then, InGaN MQWs are grown by using the lattice-matched AlInGaN as the barrier layers. The PL spectra of InGaN/AlInGaN MQWs are investigated by comparing with those of conventional InGaN/GaN strained MQWs. The results show that the use a lattice-matched AlIn-

*Project supported by the National Natural Science Foundation of China (Grant Nos. 61274003, 61422401, 51461135002, and 61334009), the Natural Science Foundation of Jiangsu Province, China (Grant Nos. BY2013077, BK20141320, BE2015111, and BK20161324), the Program for New Century Excellent Talents in University, China (Grant No. NCET-11-0229), and the Special Semiconductor Materials and Devices Research Funds from State Grid Shandong Electric Power Company, China.

†Corresponding author. E-mail: pchen@nju.edu.cn

© 2017 Chinese Physical Society and IOP Publishing Ltd

GaN superlattice barrier layer can effectively improve the luminescence performances of InGaN/AlInGaN MQWs.

2. Experiments

The InGaN/AlInGaN MQWs (Sample A) were prepared in a horizontal planetary MOCVD system. Trimethylgallium (TMG), Triethylgallium (TEG), Trimethylindium (TMI), Trimethylaluminum (TMA), and ammonia were used as source materials. A 25-nm-thick GaN buffer layer was grown on the *c*-plane of the sapphire substrate at 520 °C, then ramped temperature up to 1020 °C to grow a 1.5-μm unintentionally doped GaN layer. On the top of the GaN layer, a 100-nm-thick $In_{0.2}Ga_{0.8}N$ layer was deposited for relaxing the lattice constant. Then about an 80-nm-thick AlInGaN layer was subsequently grown at a constant temperature of 830 °C, which consists of a twenty-period AlGaN/InGaN superlattice in which each component layer thickness is less than 2 nm. The conclusions proposed in our previous report have shown that the growth temperature of 830 °C is optimal for fabricating the AlInGaN.[16] The AlInGaN layer was designed to match with InGaN well, and served as a growth template for growing the MQWs next. The MQWs consist of three InGaN wells surrounded by four lattice-matched AlInGaN barriers. The flow rates of TEG, TMA, and TMI for AlInGaN superlattice barriers were 70.8, 108, and 43.2 μmol/min, respectively. The flow rates of TEG and TMI for the InGaN well were 70.8 and 79.4 μmol/min, respectively. The structural schematic of Sample A is shown in Fig. 1. For reference, a conventional four-pair InGaN/GaN MQWs (Sample B) was also grown under a similar growth condition.

The crystal quality of the InGaN/AlInGaN MQWs is investigated by x-ray diffraction (XRD) and the surface morphology is investigated by scanning electron microscopy (SEM). The optical behaviors of the InGaN/AlInGaN MQWs are investigated by excitation-dependent PL and temperature-dependent PL.

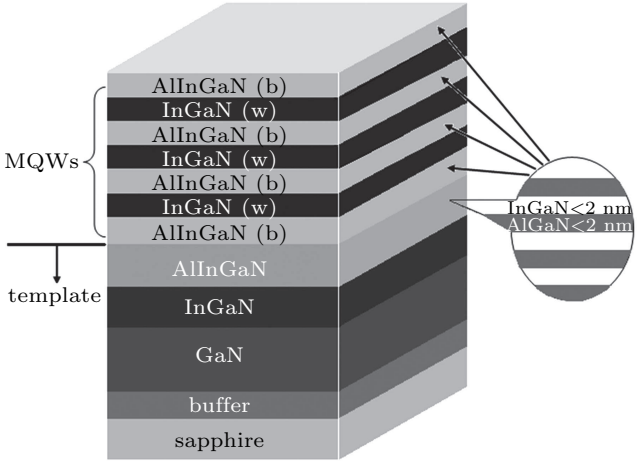


Fig. 1. Schematic of the InGaN MQWs by using AlGaN/InGaN superlattice barrier.

3. Results and discussion

Figure 2(a) shows XRD (0002) ω-scans for Sample A. Besides the diffraction peaks arising from GaN and InGaN layers, it is found that the zero-order peak of the AlGaN/InGaN superlattices overlaps with that of InGaN. This observation indicates that the out-of-plane lattice constant *c* of AlGaN/InGaN superlattice matches well with that of InGaN. For a simple biaxial strain in a hexagonal system, the out-of-plane strain $\varepsilon_\perp$ is related to the in-plane strain $\varepsilon_\parallel$ by the Poisson ratio *v*[17]

$$\varepsilon_\perp = \frac{c - c_0}{c_0} = -\frac{2v}{1-v}\left(\frac{a-a_0}{a_0}\right) = \varepsilon_\parallel,$$

where *c* and *a* are the measured strained parameters, and c_0 and a_0 are the relaxed parameters. Accordingly, free from the effects of strain, a consistent one-to-one match exists between the out-of-plane lattice constant *c* and in-plane lattice constant *a* due to the definition of Poisson's ratio *v*, i.e., both AlGaInN and InGaN are from the same material group. In a strain-free state, if the *c* values reach an identical value, then the *a* values also reach an identical value. Hence, only the main peak of the MQW can be observed around 33.9 degree without other MQW satellite peaks because of the same lattice constants between the InGaN well and the AlGaInN barrier. It is also noted that the superlattice satellite peaks can be observed between the GaN and the InGaN peaks, which indicates the smooth interface between the InGaN layer and the AlGaN layer in the superlattice structure. As shown in Fig. 2(b), in the case of a conventional InGaN/GaN MQW, the *c* values for the well and the barrier are obviously different, so the clearly resolved SL-*n* satellite peaks on each side of the InGaN SL0 peak can be observed. Meanwhile, the secondary peak between the equidistant satellite peaks can also be observed because each layer in the conventional MQWs is quite smooth. It is noted that AlGaN and InGaN component layers of the short period superlattices on the InGaN template layer involve compressive and tensile strain, respectively, because each component layer is thinner than its critical layer thickness, and thus the properly designed InGaN/AlGaN superlattices can compensate for mismatch-induced strain and be employed as the strain-compensated barrier layer for InGaN-based MQWs.[18,19] Each AlGaN or InGaN component layer is occupied simultaneously by its upper and under layer, leading to the formation of good in-plane uniformity for AlInGaN without spatial compositional (or strain) fluctuation. This is why there are no other nitrides-related peaks in XRD profiles, such as In-rich clusters. Therefore, such AlGaN/InGaN short period superlattices can be used for realizing the lattice-matched AlInGaN barriers in InGaN MQWs.

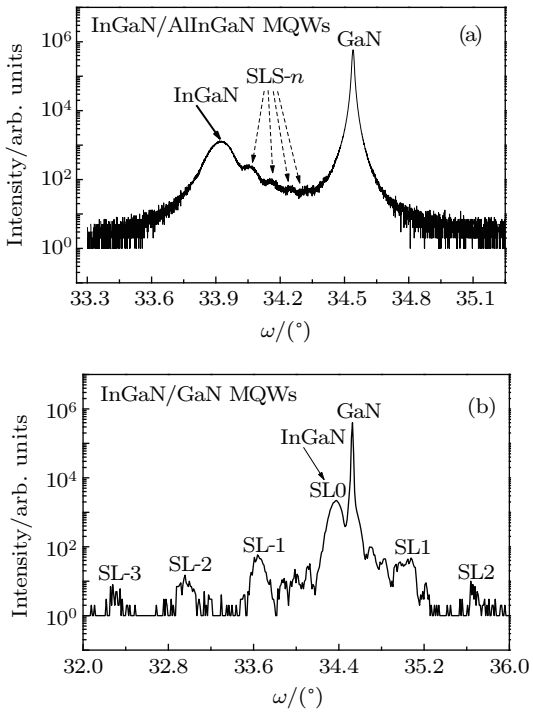


Fig. 2. XRD ω-scan profiles of (a) InGaN MQWs with lattice-matched AlInGaN barrier and (b) conventional InGaN/GaN MQW.

The surface morphologies of Samples A and B are investigated by SEM. As shown in Fig. 3(a), three V-pits can be found on the surface of the InGaN/AlInGaN MQWs, corresponding to a defect density of 4.6×10^5 cm^{-2}, which is far less than that shown in Fig. 3(b) for that of the conventional InGaN/GaN MQWs. It is known that the generations of the V-pits in InGaN are due to the In atoms congregating in the dislocation core areas under the misfit strain. Further, the In segregation, behaving as differential surfactant, reduces the surface energy of the $\{1011\}$ plane relative to $\{0001\}$ and promotes the V-pits to form a threading dislocation.[20,21] Therefore, the magnitude of strain in the MQWs directly affects the number of V-pits. From Fig. 3(a), the significant decrease of V-pit density occurs, indicating the effective suppression of overall strain in the InGaN/AlInGaN MQWs, which can be deemed as a result of the AlInGaN superlattice barrier, resulting in the elimination of driving forces for the formation of V-pits and thus the V-pits themselves.

To better understand the effect of strain on the optical properties of the two InGaN MQWs, the excitation-dependent PL measurements for Samples A and B are performed at room temperature. The PL peak positions are plotted versus excitation power in Fig. 4. The highest excitation power density is 4×10^2 W/cm^2. With the increase of excitation power, a large blueshift of nearly 10 nm is observed for Sample B. This optical behavior is familiar to that of typical strained InGaN MQWs.[22–24] As is well known, the spontaneous polarization fields in GaN and InN are approximately equal. The spontaneous polarization discontinuity is proved to be existent at the heterojunction interface of the multi-layer structure, which results in a smaller residual spontaneous polarization. Thus, it is expected that the polarization field will arise primarily from the piezoelectric effect.[25] The screening of the piezoelectric field-induced quantum confined Stark effect (QCSE) due to more photo-excited carriers causes the PL peak to be blue shifted with increasing excitation power.[26] The InGaN QW width d normally is 3 nm, the built-in field (F_{in}) in Sample B can be obtained from the equation: $F_{\text{in}} = \Delta E/qd$,[27] where the shift of emission peak energy is and q is the electronic charge. The F_{in} in Sample B is determined to be about 0.2 MV/cm, which is in the range of reported values. Thus, the blueshift is mainly due to the screening of QCSE. However, Sample A shows a negligible shift of the peak position in spite of the increase of excitation power, indicating no obvious built-in field in the MQWs. The observed unconventional PL behavior of Sample A can be explained by reducing the lattice mismatch between the well and barrier, which is consistent with the SEM observation. By using the AlInGaN superlattices as the barriers, we reduce the magnitude of strain and the corresponding built-in field in the InGaN/AlInGaN MQWs.

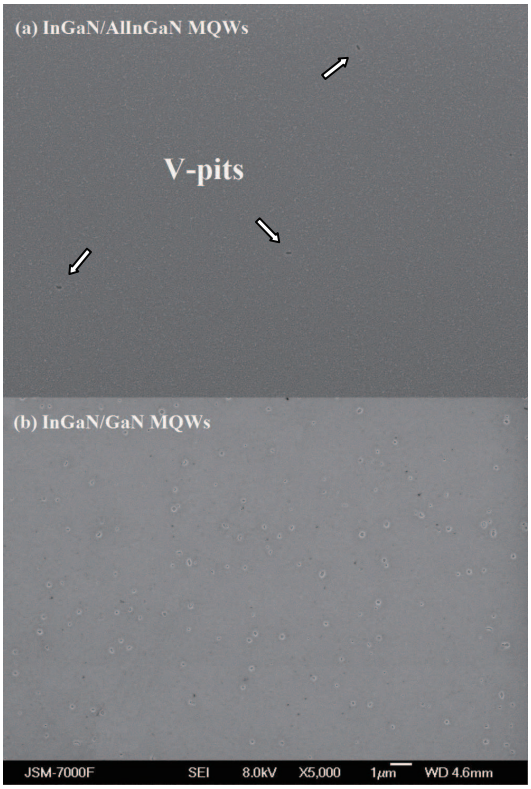


Fig. 3. SEM images for (a) InGaN/AlInGaN MQWs and (b) InGaN/GaN MQWs.

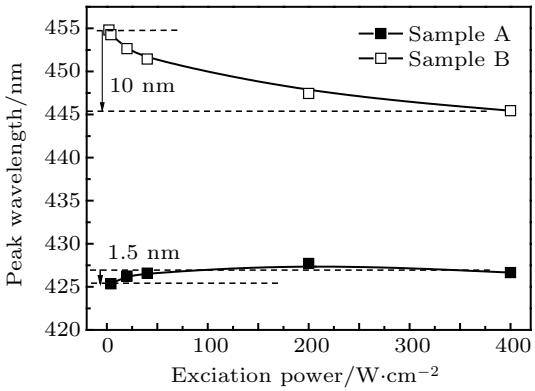


Fig. 4. Variations of PL peak position versus excitation power.

Figure 5 shows the variations of integral PL intensity with excitation power for two samples. It is noted that the integrated PL intensity of Sample B is always smaller than that of Sample A, and that the discrepancy between the two samples becomes larger, even reaches over 3 times with the increase of excitation power. As is well known, the QCSE can lead to the separation of electrons from holes,[28] and then reduce the recombination efficiency. Hence, Sample B has a strong inhibition from carriers recombining due to the built-in field. At the same time, Sample A is not influenced by the QCSE, showing a much higher PL intensity.

Meanwhile, the V-pits can serve as non-radiative recombination centers to capture carriers and also degrade the recombination efficiency of InGaN MQWs. Less V-pits in Sample A also contribute to better optical performance.

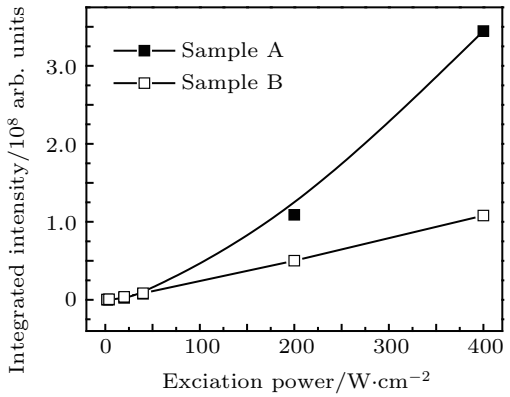


Fig. 5. Variations of integrated PL intensity with excitation power for Samples A and B.

To further investigate the luminescence mechanisms of the two samples, temperature-dependent PL experiments are performed in a closed cycle cryostat in a temperature range from 6 K to 250 K. The samples are excited by a 325-nm cw He–Cd laser. The normalized integrated PL intensities versus the reciprocal of temperature are plotted in Fig. 6, and fitted by the following Arrhenius equation:[29]

$$I(T) = \frac{1}{\left[1 + \sum a_i \exp\left(-\frac{E_{a_i}}{k_B T}\right)\right]}, \quad (1)$$

where a_i is the rate constant related to the density of non-radiative recombination centers, E_{a_i} the activation energy of the corresponding non-radiative recombination center, and k_B is Boltzmann's constant.

In Fig. 6, Sample A shows better thermal quenching behavior with the PL intensity dropping slowly as temperature increases. The thermal activation energy (E_a) extracted for Sample A is 9.3 meV, less than the exciton binding energies of most impurities,[30] which can be attributed to the slight In compositional fluctuation within InGaN wells. However, for Sample B, the PL intensity drops first slowly in the low temperature region and then more rapidly in the high-temperature region, indicating that two thermally activated non-radiative recombination centers are activated with rising temperature. As illustrated by the dash lines, two non-radiative channels are employed in the best fitting curve for Sample B. The first thermal quenching channel, with E_{a_1} of 9.6 meV and a_1 of 5.8 in the lower temperature region, similar to that for Sample A, should also be related to In compositional fluctuations within MQWs. The other non-radiative channel in the higher temperature region, with bigger E_{a_2} and a_2 (99.7 meV, 292.5), might be related to strain-induced dislocations (i.e., V-pits) because of the large value of rate constant. It is found that a_2 is much bigger than that reported in green-emitting MQWs, 53.8,[31] indicating that there are more non-radiative centers in Sample B.

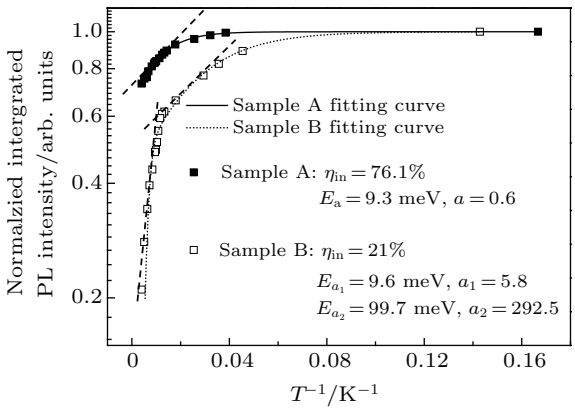


Fig. 6. Arrhenius plots of integrated PL intensity for MQWs with AlInGaN and GaN barriers.

Temperature-dependent PL experiments under a certain excitation power are also employed to estimate the internal quantum efficiency (η_{in}) of the MQWs. In the case that the PL intensity decreases monotonically with increasing temperature, the η_{in} is assumed to be equal to 100% when the PL intensity reaches saturation at low temperature, and η_{in} is defined as the ratio of the PL intensity at high temperature to that at low temperature.[32,33] As shown in Fig. 6, when the internal quantum efficiency (η_{in}) of the MQWs is taken as a benchmark at 6 K, η_{in} at 250 K obtained from the integrated PL intensity is 76.1% for Sample A, and only 21% for Sample B.

This result once again indicates the improved luminescence performance by adopting the AlInGaN superlattice barrier in MQWs.

4. Conclusions

In this work, we successfully fabricate lattice-matched AlInGaN superlattice barriers for InGaN MQWs by using the AlGaN/InGaN short period superlattices. By using the lattice-matched AlInGaN superlattice barrier in the MQWs, the V-pit density reduces as small as 4.6×10^5 cm^2. The excitation-dependent PL results confirm that using AlInGaN superlattice barriers can greatly reduce the strain-induced built-in field in the MQW and suppress the QCSE. The integrated PL intensity of the InGaN/AlInGaN MQWs shows a more than 3 times increment as compared with that of the normal InGaN/GaN MQWs. Temperature-dependent PL results show that internal quantum efficiency of InGaN/AlInGaN MQWs (76.1%) is much higher than that of the normal InGaN/GaN MQWs (21%). These results reveal that using the AlGaN/InGaN short period superlattices is an effective approach to fabricating a lattice-matched AlInGaN barrier for InGaN MQWs, and the performance of the MQWs can be greatly improved. This technique is promising for the realization of high-efficiency lighting devices.

References

[1] Tu P M, Chang C Y, Huang S C, Chiu C H, Chang J R, Chang W T, Wuu D S, Zan H W, Lin C C, Kuo H C and Hsu C P 2011 *Appl. Phys. Lett.* **98** 211107

[2] Neugebauer S, Metzner S, Bläsing J, Bertram F, Dadgar A, Christen J and Strittmatter A 2015 *Physica. Status. Solidi. (b)* **253** 118

[3] Liu J Z, Lin C H, Lee K Y, Wang Y L, Liao C L, Chang Y F, Ho C L and Wu M C 2015 *IEEE J. Quantum. Elect.* **51** 1

[4] Zhu M, Zhang X, Wang S, Yang H Q and Cui Y P 2014 *J. Mater. Sci.-Mater. El.* **26** 705

[5] Lee S N, Paek H S, Kim H, Kima K K, Chob Y H, Janga T and Parka Y 2008 *J. Cryst. Growth* **310** 3881

[6] Shang J S, Zhang B P, Mao M H, Cai L E, Zhang J Y, Fang Z L, Liu B L, Yu J Z, Wang Q M, Kusakabec K and Ohkawa K 2009 *J. Cryst. Growth* **311** 474

[7] Jones L M, Fagan S and Mair E A 2014 *Appl. Phys. Lett.* **104** 051258

[8] Broeck D M V D, Bharrat D, Hosalli A M, El-Masry N A and Bedair S M 2014 *Appl. Phys. Lett.* **105** 3

[9] Wang F, Li S S, Xia J B and Jiang H X 2007 *Appl. Phys. Lett.* **91** 061125

[10] Cai J H, Sun H Q, Zhen H, Zhang P J and Guo Z Y 2014 *Chin. Phys. B* **23** 630

[11] YU T J, Pan Y B, Yang Z J, Xu K and Zhang G Y 2007 *J. Cryst. Growth* **298** 211

[12] Pan Y B, Yu T J, Yang Z J, Wang H, Qin Z X, Hu X D, Wang K, Yao S D and Zhang G Y 2007 *J. Cryst. Growth* **298** 341

[13] Liu Y, Egawa T, Ishikawa H and Jimbo T 2003 *J. Cryst. Growth* **259** 245

[14] Liu J P, Zhang B S, Wu M, Li D B, Zhang J C, Jin R Q, Zhu J J, Chen J, Wang J F, Wang Y T and Yang H 2004 *J. Cryst. Growth* **260** 388

[15] Soh C B, Chua S J, Liu W, Lai M Y and Tripathy S 2005 *Solid. State. Commun.* **136** 421

[16] Liu Q J, Shao Y, Wu Z L, Xu Z, Xu F, Liu B, Xie Z L and Chen P 2009 *Acta Phys. Sin.* **58** 7194

[17] Moram M A and Vickers M E 2009 *Rep. Prog. Phys.* **72** 036502

[18] Nishinaka J, Funato M, Kido R and Kawakami Y 2016 *Phys. Status. Solidi* **253** 78

[19] Xiong J Y, Xu Y Q, Zhao F, Song J J, Ding B B, Zheng S W, Zhang T and Fan G H 2013 *Chin. Phys. B* **22** 108505

[20] Watababe K, Yang J R, Huang S Y, Inoke K, Hsu J T, Tu R C, Yamazaki T, Nakanishi N and Shiojiri M 2003 *Appl. Phys. Lett.* **82** 718

[21] Liu W, Soh CB, Chen P and Chua S J 2004 *J. Cryst. Growth* **268** 509

[22] Liu Z H, Zhang L L, Li Q F, Zhang R, Xiu X Q, Xie Z L and Shan Y 2014 *Acta Phys. Sin.* **63** 207304 (in Chinese)

[23] Chen G F, Tan X D, Wan W T, Shen J, Hao Q Y, Tang C C, Zhu J J, Liu Z S, Zhao D G and Zhang S M 2011 *Acta Phys. Sin.* **60** 076104 (in Chinese)

[24] Cao W Y, He Y F, Chen Z, Yang W, Du W M and Hu X D 2013 *Chin. Phys. B* **22** 076803

[25] Yu E T and Manasreh O 2002 *III-V Nitride Semiconductors: Applications and Devices* (CRC Press) pp. 17–22

[26] Chen P, Chen A, Chua S J and Tan J N 2007 *Adv. Mater.* **19** 1707

[27] Zhang J P, Yang J, Simin G, Shatalov M, Khan M A, Shur M S and Gaska R 2000 *Appl. Phys. Lett.* **77** 2668

[28] Wang T, Bai J, Sakai S and Ho J K 2001 *Appl. Phys. Lett.* **78** 2617

[29] Meneghini M, Grassa M L, Vaccari S, Galler B, Zeisel R, Drechsel P, Hahn B, Meneghesso G and Zanoni E 2014 *Appl. Phys. Lett.* **104** 113505

[30] Gotz W, Johnson N M, Chen C, Liu H, Kuo C and Imler W 1996 *Appl. Phys. Lett.* **68** 3144

[31] Lai Y L, Liu C P, Lin Y H, Hsuch T H, Lin R M, Lyu D Y, Peng Z X and Lin T Y 2006 *Nanotechnology* **17** 3734

[32] Yoichi Y, Kazuto I, Takahiro K, Naohiko S, Tsunemasa T, Hiromitsu K and Hiroaki O 2008 *J. Light & Vis. Env.* **32** 191

[33] Wang X S, Ji Z W, Wang H N, Xu M S, Xu X G, Lu Y J and Feng Z H 2014 *Acta Phys. Sin.* **63** 127801 (in Chinese)